Winful, D., Cashell, K.A., Afshan, S., Barnes, A.M., Pargeter, R.J. Elevated temperature behaviour of high strength steel columns. Journal of Constructional Steel Research, 2018; 150: 392-404. Available at: https://www.sciencedirect.com/science/article/pii/S0143974X18300506

Behaviour of high strength steel columns under fire conditions

D. Winful[abc], K.A. Cashell[b], S. Afshan[b], A.M. Barnes[c] and R. J. Pargeter[c]

[a] National Structural Integrity Research Centre, Brunel University London and TWI, UK

[b] Brunel University London

[c] TWI, UK

High strength steels (HSS) are increasingly being utilised in load-bearing applications, in particular long span and high-rise structures where there are environmental and economic benefits of using this material over conventional steel grades such as S355. However, there is limited performance data and design guidance rules for the buckling behaviour of HSS under fire conditions. The current fire resistance guidelines given in design codes are typically derived from data on steels with a yield strength less than 460 N/mm^2. In this paper, a numerical modelling study, using the finite element analysis package ABAQUS, has been carried out to assess the suitability of Eurocode fire resistance design rules for HSS columns. Elevated temperature stress-strain relationships derived from experiments were used in the development of the finite element model. The models are first validated against available test results and then used to conduct a series of parametric studies to investigate the effects of variation of steel grade, cross-section slenderness and member slenderness on the elevated temperature buckling response of HSS columns. The results are compared with the Eurocode predictions and improvements to the existing design procedures are proposed.

List of notation

A	cross-section area of the structural member
A_{eff}	effective cross-sectional area
b	width of the cross-section
h	depth of the cross-section
E_a	elastic modulus
$E_{a,\theta}$	elastic modulus at temperature θ
$E_{0.2}$	tangent modulus at 0.2% proof strength
f_{cr}	elastic critical buckling stress of the most slender constitute plate element in the section
$f_{0.2p,20}$	0.2% proof strength at ambient temperature
$f_{0.2p}$	0.2% proof strength
$f_{p,\theta}$	proportional limit at temperature θ
$f_{1.0p}$	1.0% proof strength
f_y	nominal or design yield strength
$f_{y,20}$	effective yield strength based on 2% total strain at ambient temperature θ (20°C)
$f_{y,\theta}$	effective yield strength based on 2% total strain at temperature θ
$k_{0.2p,\theta}$	the reduction factor for the 0.2% proof strength at steel temperature θ
$k_{y,\theta}$	the reduction factor for the effective yield strength at steel temperature θ
$k_{Ea,\theta}$	the reduction factor for elastic modulus at steel temperature θ
L	column length
m	strain hardening exponent determined from the points ($f_{0.2p}$, $\varepsilon_{0.2p}$) and ($f_{1.0p}$, $\varepsilon_{1.0p}$).
n	strain hardening exponent
$N_{b,fi,tRd}$	the design buckling resistance at time t of a compression member
r_i	internal radius of curvature
t	thickness of cross-section
α	imperfection factor
$\gamma_{M,fi}$	the partial safety factor, for fire situation the recommended value is 1.0

ε	parameter used to determine cross section classification or strain
$\varepsilon_{0.2p}$	total strain at 0.2% proof strength $f_{0.2p}$
$\varepsilon_{1.0p}$	total strain at 1.0% proof strength $f_{1.0p}$
ε_{nom}	engineering strain
ε_{pl}^{ln}	log plastic strain
$\varepsilon_{p,\theta}$	strain at the proportional limit
$\varepsilon_{t,\theta}$	limiting strain for yield strength
$\varepsilon_{y,\theta}$	yield strain
$\varepsilon_{u,\theta}$	strain at ultimate tensile strength
θ	temperature
σ	stress
σ_{nom}	engineering stress
σ_{true}	true stress
$\bar{\lambda}$	non-dimensional slenderness at ambient temperature
$\bar{\lambda}_{\theta}$	non-dimensional slenderness at temperature θ
φ_{θ}	parameter used to calculate χ_{fi}
χ_{fi}	the reduction factor for the flexural buckling in the fire
ω_0	local imperfection amplitude

1 Introduction

This paper is concerned with the behaviour of columns made from high strength steel in fire conditions. High strength steels (HSS) are defined herein as steel grades with a yield strength between 460 and 700 N/mm^2 in accordance with Eurocode 3 Part 1-12 [1]. These grades are increasingly being utilised in structural applications, in particular for long span structures and high-rise buildings where there are environmental and economic benefits of using these grades over conventional steel grades (e.g S355). The higher strength of these materials compared with mild steel can result in smaller section sizes and less material being required for members where strength rather than deflection governs the design. As a consequence, there may be benefits in terms of reduced foundation sizes, less transportation and handling costs and an overall reduction in the environmental impact of the construction.

Despite their increasing popularity, one of the main barriers to more widespread use of HSS in construction is a lack of usable design information which allows designers to fully harness their advantages. In this context, and owing to the ever-increasing demands for more sustainable construction, there has been an increase in research activity on the subject of HSS structures in recent years including major European collaborative projects [2,3], as well as studies into beams [4], columns [5,6] and also different extreme loading scenarios [7–9].

In the case of a fire, structures should meet the legal requirements for fire resistance (i.e. the ability of a structure to maintain its function for a prescribed amount of time in a fire [10]), and this involves having an understanding of how structural elements perform in such an event. There is a considerable amount of information in the literature on the buckling behaviour of conventional steel grades at elevated temperatures [11–13]. Most of this work, which includes experiments and numerical modelling, has contributed towards the current structural fire design guidelines given in Eurocode 3 Part 1-2 [14]. Although the Eurocode was derived from data on steels with yield strengths less than

460 N/mm^2, these guidelines are currently applicable to HSS with no additional design comments. Further research is necessary to assess the applicability of these design rules, specifically to ensure the standards are reliable and economical. To date, there are very limited performance data and studies on the buckling behaviour of HSS columns under fire conditions [15–17], mainly owing to the significant expense associated with high temperature structural testing as well as the lack of reliable material properties which are needed for analysis and design [18].

In this paper, a numerical study is carried out to investigate the structural performance and design of high strength steel columns for fire conditions. The paper proceeds with a discussion on the metallurgical characteristics, in particular the strengthening mechanisms employed, and the various production routes used to produce HSS and will also comment on how these are affected by temperature. The various mathematical representations of the stress-strain response are described and the modified Ramberg-Osgood model proposed by Gardner and Nethercot [19] is used to characterise the stress-strain response of S690QL and S700MC at elevated temperatures, obtained from a previous study [20]. Results from that experimental study showed that S700MC has better strength retention properties than S690QL at temperatures up to 800°C, mainly owing to the alloying content and production route of these steels. S700MC is thermomechanically control processed (M) and suitable for cold forming (C), whilst S690QL is quench and tempered (Q) and meets the minimum impact energy of 30 J at -40°C (L). Finally, the general purpose finite element analysis software ABAQUS [21] is used to develop and validate numerical models for predicting the ultimate loads of the columns at ambient and elevated temperatures. A parametric study is then conducted, which incorporates the elevated temperature stress-strain relationships of S690QL and S700MC. The aim of this study is to generate data on the structural performance of Class 1 and Class 3 columns made from these steel grades at temperatures up to 800°C and assess the suitability of the Eurocode buckling curves [14] for HSS columns in fire conditions.

2 Material and metallurgical properties of high strength steels

2.1 Strengthening mechanisms

There are a number of different strengthening mechanisms used to make high strength steels. Most of these involve restricting or reducing the movement of metallographic imperfections known as dislocations through the material. Plastic deformation is due to the movement of these dislocations and so, by restricting their mobility, the dislocations require more stress to move, resulting in an increase in yield strength. The dislocation movement can be slowed down by the presence of alloying elements in the form of solute atoms (e.g. molybdenum) or precipitates (e.g. molybdenum carbides), grain boundaries or other dislocations. Commercial grades of HSS are typically strengthened through a combination of mechanisms rather than just one isolated approach. The most commonly employed of these strengthening mechanisms, as well as how they are affected by elevated temperature, are summarised as:

- *Grain refinement*: the process of producing a microstructure with fine grains which, in turn, results in more grain boundaries. In general, between 400–700°C, grain growth occurs which

reduces the amount of grain boundaries. However, it has been shown that the yield strength becomes almost independent of grain size at temperatures above 600±50°C [22].

- *Solid solution strengthening*: by distorting the iron crystal lattice, the movement of dislocations is reduced resulting in an increase in yield strength. It has been shown [23] that solid solution strengthening does not adversely affect the ductility and is largely unaffected by temperature.
- *Precipitation hardening*: this method differs from solid solution strengthening in that the increase in yield strength is due to the precipitates directly obstructing the motion of dislocations as opposed to indirectly through distorting the iron crystal lattice. Chromium, molybdenum, niobium, vanadium, tungsten and titanium carbonitrides used in steel form at about 500–650°C [24] and, hence, precipitation hardening is a useful strengthening mechanism at elevated temperature [23].
- *Strain hardening*: this is when dislocations are introduced into the crystal lattice through plastic strain. Since dislocations are obstacles to each other, an increase in the dislocation density leads to an increase in strength. Recovery occurs at elevated temperature where the amount of dislocations introduced through plastic strain is reduced and so the impact of this strengthening mechanism reduces [25].

2.2 Production routes

In addition to the different strengthening methods, high strength steels are produced in different ways using various heat treatments and rolling regimes to manipulate the microstructure and achieve the optimal properties for a given application. Alloying elements, such as carbon, manganese, molybdenum, niobium and vanadium also play an important role in manipulating the microstructure through the different strengthening mechanisms mentioned previously. HSS are traditionally hot rolled in the austenitic region which is typically above 900°C but this temperature is dependent on the chemical composition. The steel is then cooled at different rates to get the desired mechanical properties. The steel grades for structural steels in Europe are denoted by an S at the beginning of their designation followed by the minimum yield strength in N/mm^2 and then the production route/delivery condition, where N, Q, M and C are used for materials that are normalised (N), quench and tempered (Q), thermo-mechanically rolled or thermo-mechanically control processed (M) and cold-formed (C), respectively.

2.3 Stress-strain relationship in design

Many advanced calculation methods such as finite element analysis require the full stress-strain response of a material to accurately depict the structural behaviour at ambient and elevated temperatures. Various mathematical relationships exist to capture this behaviour which are discussed hereafter.

2.3.1 Ambient temperature

Eurocode 3 Part 1-1 [26] adopts a bilinear stress-strain response for mild steel at ambient temperature. In this case, the response of the steel is assumed to be linear-elastic up to the yield point (f_y) and then exhibits a yield plateau as illustrated in Fig. 1.

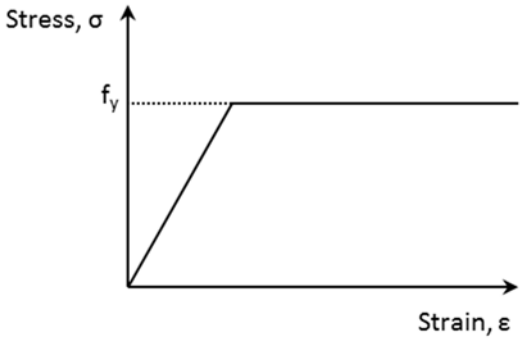

Figure 1 Bi-linear stress-strain relationship

2.3.2 Elevated temperature

At elevated temperature, it is noted that the stress-strain relationship becomes increasingly non-linear, that is, the linear elastic region reduces and becomes difficult to distinguish from the non-linear plastic region. Similar to the Eurocode approach for ambient temperature design, multi-linear functions can be used to approximate the stress-strain behaviour. Although this method simplifies the stress-strain behaviour, it is acceptable to use when deformation does not play a significant role and only the load-carrying capacity is critical for design. To get an accurate representation of the stress-strain behaviour, a large number of data lines are required [27].

Eurocode 3 Part 1-2 [14] adopts Rubert and Schaumann's [28] model derived from anisothermal tests on beams. This is a four-stage material model, as depicted in Fig. 2. With reference to this figure, the first stage is a linear elastic region defined by a temperature dependent gradient (elastic modulus, $E_{a,\theta}$) up to the proportional limit ($f_{p,\theta}$), which is defined as the point where the curve changes from elastic to plastic. The second stage begins at the proportional limit ($f_{p,\theta}$) and is graphically represented as an elliptical curve up until the maximum strength ($f_{y,\theta}$) is achieved at a strain of $\varepsilon_{y,\theta}$ (2%). In the third stage, a constant strength is assumed between $\varepsilon_{y,\theta}$ and $\varepsilon_{t,\theta}$ (which is defined in the Eurocode as 15%) and at the fourth stage the stress drops to zero at the ultimate strain $\varepsilon_{u,\theta}$ (20% in the Eurocode). An alternative stress-strain relationship, which incorporates strain hardening for temperatures below 400°C, is provided in Annex A of Eurocode 3 Part 1-2 [14].

A disadvantage of this model is that the rate of change of gradient (i.e. the curvature) from the proportional limit ($f_{p,\theta}$) and yield ($f_{y,\theta}$) points are not continuous [29]. The elliptical curve used to characterise the stress-strain response at elevated temperature has been shown to overestimate the stress-strain response of some high strength steels including S460N and S460M [30], HSA800 (S650M) [31] as well as RQT 701 [32]. Consequentially, these limiting factors may result in the overestimation of the buckling capacity of steel element in a fire scenario.

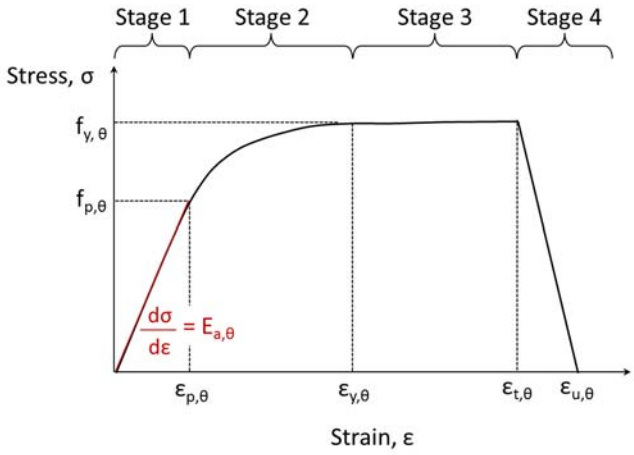

Figure 2 Stress-strain model for steel at elevated temperature as shown in Eurocode 3 Part 1-2 [14]

A popular choice amongst researchers is the modified Ramberg-Osgood model, which has been used to characterise the stress-strain response of various HSS [e.g. 15,31,33] at elevated temperature. The original Ramberg-Osgood model [34], which was later modified by Hill [35], is presented in Eq. 1:

$$\varepsilon = \left(\frac{\sigma}{E_a}\right) + 0.002\left(\frac{\sigma}{f_{0.2p}}\right)^n \quad (1)$$

where σ and ε are the engineering stress and strain, respectively, E_a is the elastic modulus, $f_{0.2p}$ is the 0.2% proof strength and n is the strain hardening exponent, which describes the curvature of the stress-strain curve (i.e. the lower the value of n, the more gradual the transition from linear to non-linear part of the stress-strain curve).

Compound Ramberg-Osgood models have been proposed by Mirambell and Real [36], Ramussen [37] and Gardner and Nethercot [19], where different portions of the stress-strain curve are modelled using separate Ramberg-Osgood models. Mirambell and Real's proposal was limited to tensile applications since the tensile strength and strain are used. Gardner and Nethercot's model uses the 1.0% proof strength ($f_{1.0p}$) and corresponding strain ($\varepsilon_{1.0p}$) instead of the tensile strength to make the model applicable in both tension and compression applications and achieve greater accuracy at strains of general interest in structural applications (i.e. up to 10%) [19].

In the model proposed by Gardner and Nethercot [19], Eq. 1 is used to characterise the stress-strain curve up to and including the 0.2% proof strength ($f_{0.2p}$). For stresses greater than the 0.2% proof strength, Eq. 2 is used:

$$\varepsilon = \left(\frac{\sigma - f_{0.2p}}{E_{0.2}}\right) + \left(\varepsilon_{1.0p} - \varepsilon_{0.2p} - \frac{f_{1.0p} - f_{0.2p}}{E_{0.2}}\right) \times \left(\frac{\sigma - f_{0.2p}}{f_{1.0p} - f_{0.2p}}\right)^m + \varepsilon_{0.2p} \text{ for } \sigma > f_{0.2p} \quad (2)$$

where $E_{0.2}$ is the slope at 0.2% proof strength and m' is the strain hardening exponent determined from the points ($f_{0.2p}$, $\varepsilon_{0.2p}$) and ($f_{1.0p}$, $\varepsilon_{1.0p}$).

Gardner and Nethercot's [19] adaptation of the Ramberg-Osgood model (Eqs. 1 and 2) has been applied to represent the stress-strain response of two different grades of HSS, S690QL and S700MC

which are named steels A and B hereafter, respectively, at various levels of elevated temperature. The stress-strain data for both grades was obtained from an extensive series of tensile tests, conducted at various temperatures up to 800°C; further details on these tests, including the experimental procedure, are available elsewhere [20]. The parameters for the modified Ramberg-Osgood model are presented in Tables 1 and 2. The strain hardening parameters n and m' were obtained using the ordinary least square method as described by Afshan *et al.* [38]. Examples of Eq. 1 and 2 fitted to experimental data for steels A (S690QL) and B (S700MC) are presented in Figs. 3 and 4, respectively. Generally, the modified Ramberg-Osgood model proposed by Gardner and Nethercot [19] closely traces the stress-strain response of steels A (S690QL) and B (S700MC) within this temperature range. The transition from linear to non-linear is more pronounced for steel A (S690QL) than steel B (S700MC) at temperatures below 400°C as demonstrated through the higher strain exponent, n, in Tables 1 and 2.

All variations of the modified Ramberg-Osgood model, including Eqs. 3 and 4, are only capable of tracing the stress-strain response up to the tensile strength (i.e. maximum strength before necking occurs), as shown in Figs. 3 and 4. The model cannot account for strain softening, which may be relevant in applications where high strains are important such as in the case of fire where anticipated strains may be greater than 2%. Nevertheless, at 600°C for steel A (S690QL), as well as 700 and 800°C for steel B (S700MC), the ultimate strength was reached at strains less than 2%.

Table 1 Summary of the parameters for the modified Ramberg-Osgood model proposed by Gardner and Nethercot [19] for steel A (S690QL)

Temperature, θ (°C)	E_a (GPa)	$E_{0.2}$ (GPa)	$f_{0.2p}$ (N/mm^2)	$f_{1.0p}$ (N/mm^2)	n	m'
20	199.29	3.41	706.33	717.34	101.98	1.52
100	189.70	10.01	690.00	707.96	32.50	1.52
200	191.16	9.71	667.50	688.78	32.23	1.78
300	183.35	14.89	651.00	699.59	20.08	2.39
400	176.67	16.92	643.00	673.09	16.52	2.88
500	178.00	13.59	567.00	610.21	19.03	5.17
600	149.71	15.21	442.00	499.94	14.07	3.15
700	76.27	9.99	222.50	249.19	9.74	7.62
800	53.74	4.05	70.00	80.06	7.97	3.75

Table 2 Summary of the parameters for the modified Ramberg-Osgood model proposed by Gardner and Nethercot [19] for steel B (S700MC)

Temperature, θ (°C)	E_a (GPa)	$E_{0.2}$ (GPa)	$f_{0.2p}$ (N/mm^2)	$f_{1.0p}$ (N/mm^2)	n	m'
20	224.69	24.52	749.33	793.30	13.77	2.40
100	204.63	24.82	744.00	768.96	13.08	2.03
200	217.55	21.37	703.00	749.20	14.80	2.80
300	210.53	26.05	735.00	798.48	12.28	4.17
400	205.57	25.94	691.00	770.08	11.54	3.41
500	190.11	19.16	610.00	672.69	14.34	4.00
600	178.25	23.77	511.50	559.70	9.34	6.86
700	140.76	14.29	350.00	367.35	10.96	3.91
800	86.74	5.51	175.00	179.82	14.87	1.74

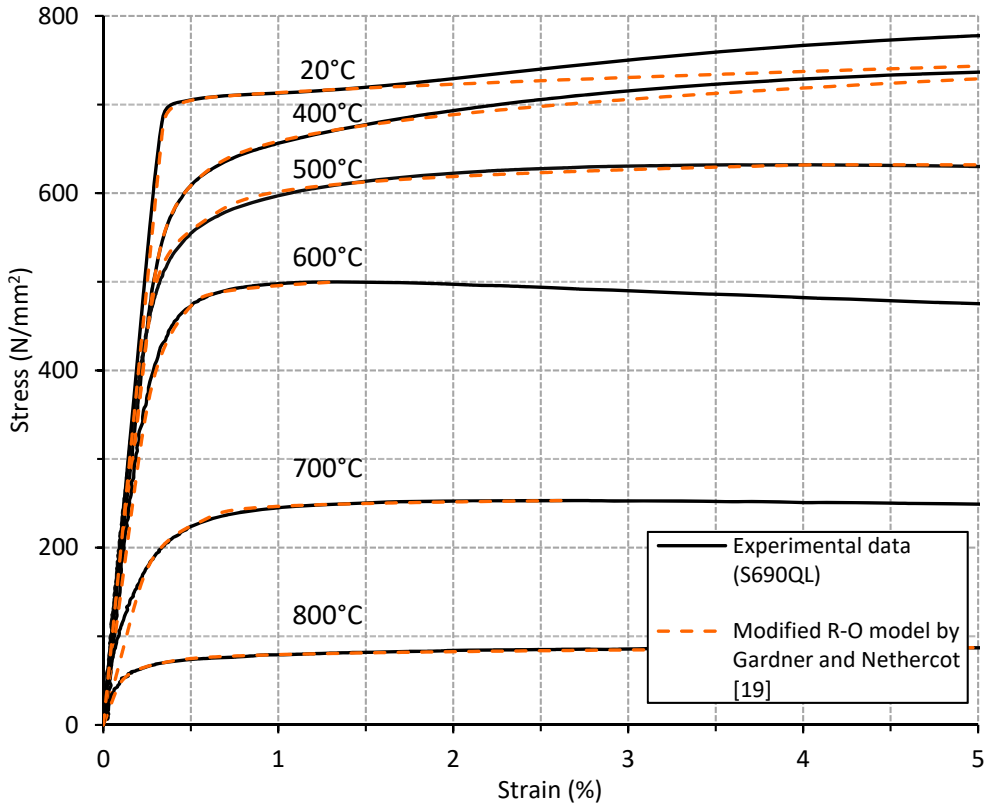

Figure 3 Comparisons of the stress-strain response for steel A (S690QL) with the modified Ramberg-Osgood model proposed by Gardner and Nethercot [19]

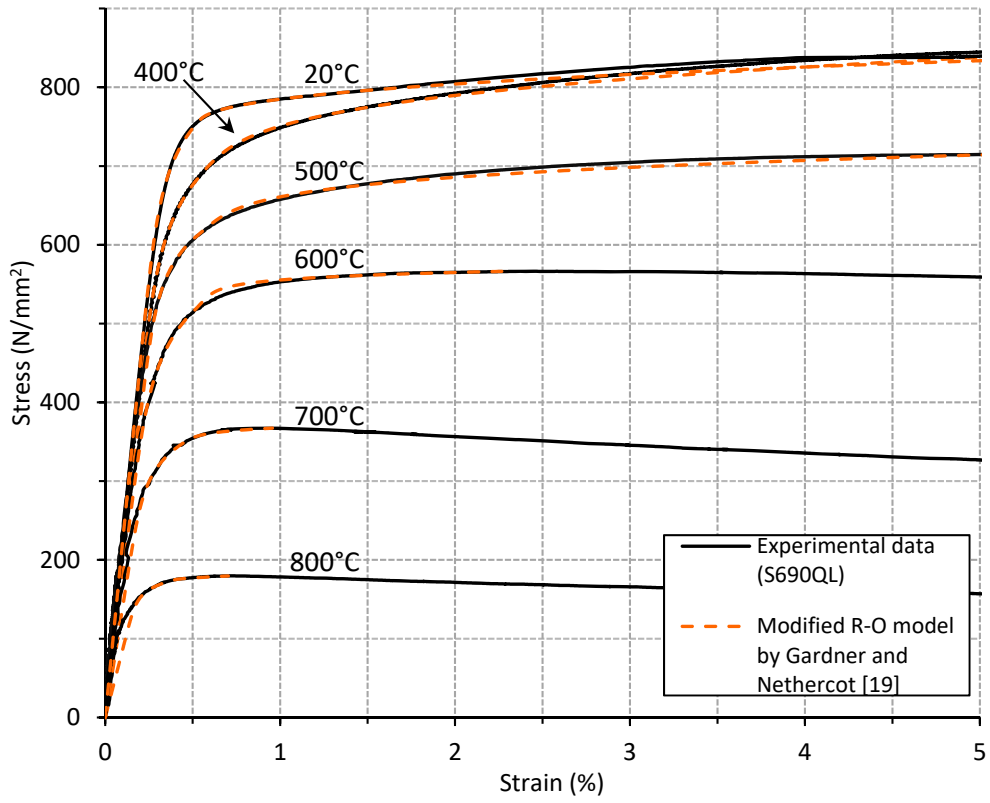

Figure 4 Comparisons of the stress-strain response for steel B (S700MC) with the modified Ramberg-Osgood model proposed by Gardner and Nethercot [19]

3 Development of the numerical model

A three-dimensional finite element (FE) model has been developed using the general purpose ABAQUS software [21] to investigate the behaviour of high strength steel columns at elevated temperature, utilising the material information described previously. The ABAQUS software was selected as it is commercially-available and is capable of depicting the material and geometric nonlinearities as well as the elevated temperature behaviour accurately [9]. In the following sub-sections, the development of the model is described. This is followed by an account of the validation exercise where the model is compared with experimental results.

3.1 General

At ambient temperature, there are two stages to the numerical analysis, (1) a linear elastic buckling analysis using the **BUCKLE* procedure in ABAQUS to determine the buckling mode shape, and (2) a geometrically and materially nonlinear load-displacement analysis, incorporating the buckling mode shape as an imperfection from stage (1). The stage (2) stress analysis is completed using the modified Riks method, which is a variation of the classic arc length method and enables the buckling behaviour to be examined as the structural member undergoes large deformations under an applied load. At elevated temperature, the columns are modelled isothermally, whereby the initial temperature is set to the target temperature θ using the predefined field. Although this is not necessarily representative of a real fire scenario in which the members would heat up in an anisothermal manner, the isothermal test conditions have been commonly used by researchers [9,13,39] for numerical and experimental studies as they tend to provide a reliable and controllable approach, making validation more straightforward with the result given as an ultimate load for a given temperature [9]. The Abaqus/Standard analysis method is used in this study.

3.2 Material properties

ABAQUS requires the material stress-strain curves to be specified in terms of true stress σ_{true} and log plastic strain ε_{pl}^{ln} which are derived from the nominal engineering stress-strain curves using Eq. 3 and 4, respectively, where σ_{nom} and ε_{nom} are the engineering stress and strain, respectively, and E_a is the elastic modulus. Poisson's ratio is taken as 0.3 at ambient and elevated temperatures in accordance with Eurocode 3 Part 1-1 [26]. It has been shown that Poisson's ratio gradually increases from 0.285 to 0.315 between 20 and 800°C [40] and therefore a value of 0.3 is reasonable and adopted in the model. The alloying content and microstructure has minimal influence on Poisson's ratio and so it is assumed that this value can be used to model both conventional and HSS grades [41].

$$\sigma_{true} = \sigma_{nom}(1 + \varepsilon_{nom}) \quad (3)$$

$$\varepsilon_{pl}^{ln} = \ln(1 + \varepsilon_{nom}) - \frac{\sigma_{true}}{E_a} \quad (4)$$

3.3 Boundary conditions and load application

The model assumes that the column is symmetric, both in terms of geometry and the boundary conditions. Hence, only half of the cross-section over half of the column length is included in the finite element model. The test boundary conditions are replicated by restraining the appropriate displacement and rotation degrees of freedom at the column ends. All boundary conditions are applied through reference points at these locations. At ambient temperature, the columns are pin-

ended so all degrees of freedom of the lower reference point, except rotation about one axis, are fixed, while the upper reference point is free to displace along the column axis and rotate about the same axis as the lower reference point.

At elevated temperature, the stub and slender columns have fixed- and pin-ended conditions, respectively. For the fixed-ended columns, all six degrees of freedom of the lower reference point are restrained, while the upper reference point is allowed to move longitudinally along the column axis and is fixed against the other five degrees of freedom. The elevated temperature pin-ended columns are modelled in the same way with the exception that the rotation axis is set as the minor axis in all cases. All columns are concentrically loaded through their upper reference point.

3.4 Geometric imperfections, residual stresses and mesh size

All structural members contain geometric imperfections which are introduced during production, fabrication and handling. Initial imperfections in the form of the lowest local and global buckling mode, obtained from a linear elastic eigenvalue buckling analysis, are included in the models. The amplitude of the imperfection is set to replicate the values given during test programmes [13,42], which are used later for validation. Residual stresses, similarly introduced during manufacturing (e.g. cold-forming) or welding, are not explicitly incorporated into the models due to their low measured amplitudes and minimal influence on the member compressive resistance in similar material [42]. Shell elements are adopted to simulate HSS tubular hollow section columns as have been adopted in similar studies (e.g [15,42]). The four-noded shell elements with double curvature and reduced integration (S4R) are employed in all the FE models. Based on a mesh sensitivity assessment, the model employed a mesh comprising cubic elements whereby the size of the elements was equal to the thickness of the section under consideration. This was found to provide an efficient solution without compromising the accuracy of the simulation.

4 Validation of the numerical model

In the absence of elevated temperature tests on HSS columns in the literature, the finite element (FE) models are validated against (1) the ambient temperature experiments on high strength steel columns reported by Wang and Gardner [42] and (2) the elevated temperature tests on columns made from mild steel reported by Pauli *et al.* [13]. Both test programmes included measurements of material properties, geometry as well as local and global geometric imperfection amplitudes of the tested columns. The same modelling procedures are employed for both the room temperature and elevated temperature tests by incorporating the material properties corresponding to the test temperature under consideration.

4.1 Ambient temperature response

Wang and Gardner [42] conducted a series of tests on S460N and S690Q hot-finished HSS square hollow section columns which were pinned at both ends and allowed in-plane rotation of the member about one axis only. The columns were loaded under displacement control at a loading rate of $L_{cr}/2000$ per minute, where L_{cr} is the buckling length taking into account the member length (L) plus 150 mm to account for the distance between the knife-edge supports used to simulate the pin-ended boundary conditions. A summary of the details from the test programme is presented in Table 3, which includes the failure load measured during the test ($N_{u,test}$). Tensile coupon tests on material extracted from the

flat faces of the S460N and S690Q columns were performed to measure their basic engineering stress-strain response and these are incorporated into the FE models, once converted to true stress and strain using Eq. 3 and 4.

Table 3 Summary of the test conditions reported by Wang and Gardner [42] at ambient temperature

Specimen	Steel grade	Nominal section size (mm)	L (mm)	$N_{u,test}$ (kN)	$N_{u,FE}$ (kN)	$N_{u,test}$ / $N_{u,FE}$
C3L1	S460N	100 × 100 × 5	708	878	888	0.99
C3L2	S460N	100 × 100 × 5	1609	798	850	0.94
C3L3	S460N	100 × 100 × 5	2799	557	576	0.97
C4L1	S690Q	50 × 50 × 5	276	690	705	0.98
C4L2	S690Q	50 × 50 × 5	518	637	588	1.08
C4L3	S690Q	50 × 50 × 5	756	562	520	1.08
C4L4	S690Q	50 × 50 × 5	1070	391	360	1.09
C4L5	S690Q	50 × 50 × 5	1379	248	230	1.08
C4L6	S690Q	50 × 50 × 5	1550	201	195	1.03
C4L7	S690Q	50 × 50 × 5	1710	166	165	1.01
C4L8	S690Q	50 × 50 × 5	2000	119	126	0.94
C5L1	S690Q	100 ×100 × 5.6	709	1571	1608	0.98
C5L2	S690Q	100 ×100 × 5.6	1609	1420	1376	1.03
C5L3	S690Q	100 ×100 × 5.6	2800	680	679	1.00

Fig. 5 shows the load-lateral deflection curves derived from the numerical models of the C4L6 and C5L3 members which are compared with their respective test responses. These models are selected for demonstration purposes and similar graphs have been obtained for all other columns. The numerical model is observed to provide an accurate depiction of the load-deformation history of the high strength steel columns. A summary of the comparisons between the ultimate test load ($N_{u,test}$) and ultimate FE load ($N_{u,FE}$) reached is provided in Table 3, as well as the ratio of these two figures. It is shown that the FE model gives a mean $N_{u,test}/N_{u,FE}$ value of 1.01 and a COV of 5.0%. From the results provided in Table 3 it is concluded that the FE model is adequate of predicting the ultimate strengths of HSS columns at ambient temperature.

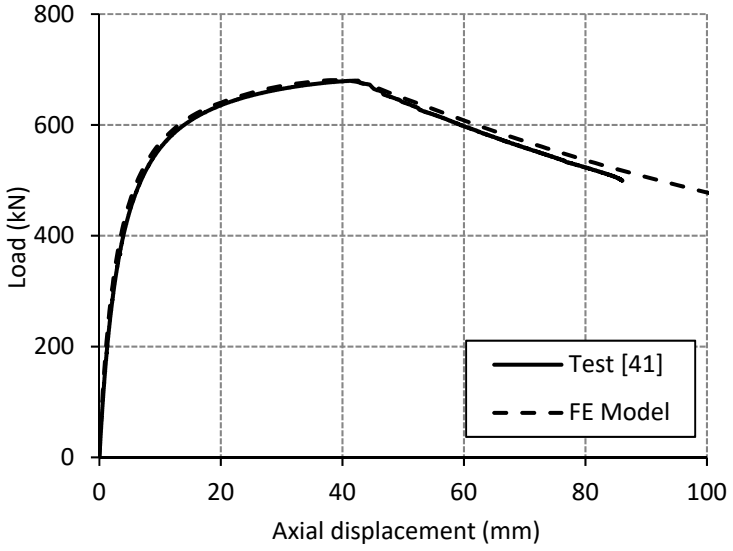

(a)

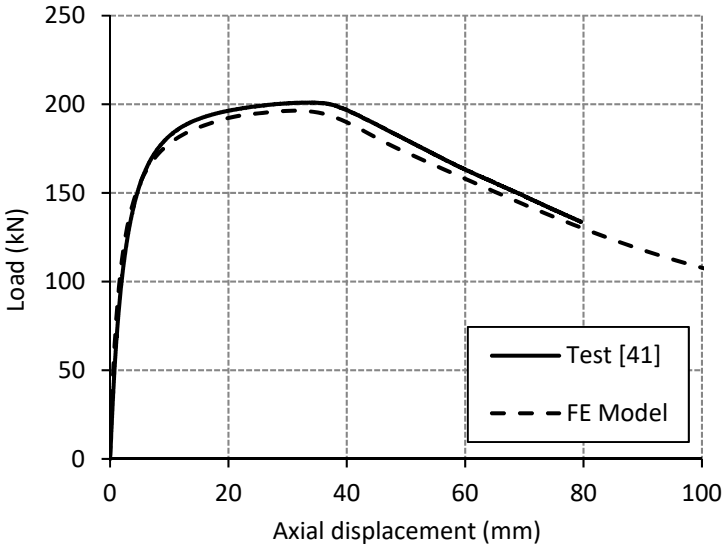

(b)

Figure 5 Comparison of the load–lateral displacement curves for the (a) C4L6 and (b) C5L3 HSS columns [42]

4.2 Elevated temperature response

The FE model described previously is employed to analyse the columns tested by Pauli *et al.* [13]. Although these experiments were conducted on columns made from conventional S355 steel, they are used in the current paper for validation of the model owing to a lack of experimental results for HSS columns in fire. This test programme included tests on square and rectangular hollow sections (SHS and RHS, respectively), and included both stub and long columns. All members were made of S355 hot-finished sheets which were rolled into shape at ambient temperature and welded closed. The experiments were performed under isothermal loading conditions whereby the columns were first heated to a target temperature of 400, 550 or 700°C and then, once thermal equilibrium had been established at the desired temperature, a mechanical load was applied at a strain rate of 0.1%/min until the horizontal displacement increased rapidly and the vertical load could no longer be maintained. The details of the tests are presented in Table 4. Similarly to the ambient temperature validation, the elevated temperature model incorporates the material properties corresponding to the test temperature under consideration. In the test programme, tensile coupons were extracted from flat faces of the S355 columns and then tensile tests were conducted at ambient, 400, 550 and 700°C under isothermal conditions at a strain rate of 0.1%/min. These tests were analysed [42] and the proposed input parameters for the modified Ramberg-Osgood model as developed by Gardner and Nethercot [19] and given in Eqs. 1 and 2, are included in the FE model.

Table 4 Summary of the test conditions reported by Pauli *et al.* [13] at elevated temperature

Specimen	Nominal section size (mm)	L (mm)	θ (°C)	End-condition	$N_{u,test}$ (kN)	$N_{u,FE}$ (kN)	$N_{u,test}$ / $N_{u,FE}$
S3	160 × 160 × 5	480	400	Fixed	795	767	1.04
S6	160 × 160 × 5	480	550	Fixed	468	474	0.99
S5	160 × 160 × 5	480	700	Fixed	138	128	1.08
S02	60 × 120 × 3.6	360	400	Fixed	408	330	1.24
S03	60 × 120 × 3.6	360	550	Fixed	257	218	1.18
S06	60 × 120 × 3.6	360	700	Fixed	74	71	1.04

L2	160 × 160 × 5	1840	400	Pinned about major axis	760	701	1.08
L5	160 × 160 × 5	1840	550	Pinned about minor axis	467	443	1.05
L6	160 × 160 × 5	1840	700	Pinned about minor axis	130	119	1.10
L08	60 × 120 × 3.6	1840	400	Pinned about minor axis	242	262	0.92
L10	60 × 120 × 3.6	1840	550	Pinned about minor axis	186	165	1.13
L05	60 × 120 × 3.6	1840	700	Pinned about minor axis	71	64	1.10

In the elevated temperature test programme, the stub columns were fixed against displacement and rotation at both ends, apart from axial displacement at the loaded end, while the long columns were pinned at both ends and allowed in-plane rotation of the member about either the major or minor axis.

Comparisons of the load-vertical displacement response from the test and FE model are depicted in Fig. 6, whilst the results from the validation study are presented in Table 4 where $N_{u,test}/N_{u,FE}$ is a measure of how accurately the FE model predicts the ultimate load. For the stub columns, the FE model gives a mean $N_{u,test}/N_{u,FE}$ value of 1.09 and a coefficient of variation of 7.9%. On the other hand, for the slender columns the FE model gives a mean $N_{u,test}/N_{u,FE}$ value of 1.04 and a coefficient of variation of 8.3%. Fig. 6 demonstrates that the model fairly traces the load-deflection response of the columns; whilst Table 4 shows that the model generally underestimates the ultimate load of the columns and thus provides a safe prediction for the fire resistance of steel columns. The discrepancy is relatively small and most likely attributed to various factors such as the use of nominal dimensions (including the corner radii of the cross-section) and the mean value for the global imperfection as well as idealised boundary conditions which can be difficult to replicate experimentally. In addition, the influence of residual stresses introduced during welding are not considered in the model. In summary, from the results provided in Table 4, it is concluded that the FE model is adequate for predicting the ultimate strengths of columns made from mild steel at elevated temperature.

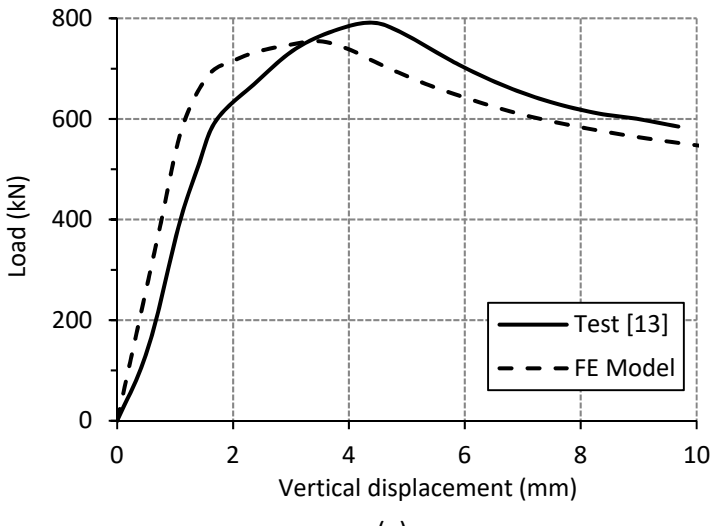

(a)

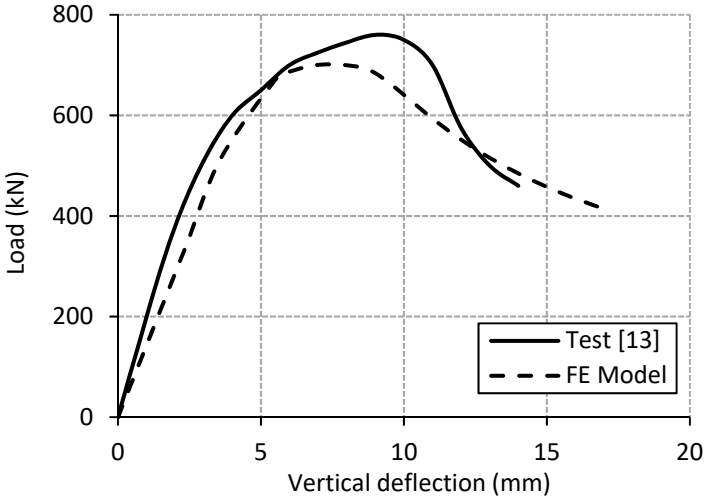

(b)

Figure 6 Comparison of the load–lateral displacement curves for column (a) S3 and (b) L2 [13]

5 Parametric study

Following the validation of the FE models, in the current section, a series of parametric studies is described which have been performed in order to generate further structural performance data to assess the suitability of the Eurocode 3 Part 1-2 [14] buckling curves for high strength steel compression members in fire. The influence of a number of salient parameters is investigated including material grade, cross-sectional geometry and member length. Two grades of HSS, namely S690QL and S700MC (steel A and steel B, respectively), are included in the study as well as four cross-section geometries with varying member lengths. The same modelling procedures as explained in the previous sections are employed in the parametric study. The temperature is applied in an isothermal manner which involves using the material properties for a given temperature (θ); the applied load is then increased until failure occurs, which is typically soon after the ultimate load has been reached. Since the influence of time-dependent effects, e.g. creep, are not included in the developed FE models, this approach is considered acceptable.

The outer dimensions of the parametric study models are selected as a 100 × 100 square hollow section and a 100 × 50 rectangular hollow section, for both grades, resulting in two different cross-section aspect ratios (i.e. h/b=1.0 or 2.0, where h is the height of the section and b is the width). The effect of cross-section slenderness is investigated by varying the cross-section thickness, while maintaining the cross-section outer dimensions. Thus, two different thicknesses are selected for each of the considered cross-sections such that one Class 1 (with a thickness of 5.6 mm) and one Class 3 (with a thickness of 4 mm) cross-section are modelled in each case, in accordance with the classification specifications in Eurocode 3 Part 1-1 [26].

For the RHS models, buckling about both major and minor axes is considered to investigate if different buckling curves are required for each case. All columns are modelled as pin-ended providing a member non-dimensional slenderness range ($\bar{\lambda}$) of 0.5 to 2.5. The measured stress-strain curves for steels A (S690QL) and B (S700MC) presented in Section 2.2 are first modified into the true stress versus log

plastic strain values before being incorporated into the models. The global imperfection amplitude is taken as L/1000, where L is the column length, in accordance with the recommendations in Eurocode 3 Part 1-2 [14]. The local imperfection amplitude (ω_0) is determined using the Dawson and Walker model [43], as has been used for a similar study on HSS members [4], and is given as:

$$\omega_0 = 0.028t\,(f_y/f_{cr})^{0.5} \quad (5)$$

where t is the thickness, f_y is material yield strength and f_{cr} is the elastic critical buckling stress of the most slender constituent plate element in the section. Owing to the symmetry in the geometry and the boundary conditions of the models, only half of the section, and half of the member length, is included in the model. An example of the deformation of the column for steel B (S700MC) obtained from the finite element analysis simulation in ABAQUS is presented in Fig. 7. The results from the parametric study are presented and discussed in the following section, together with design recommendations.

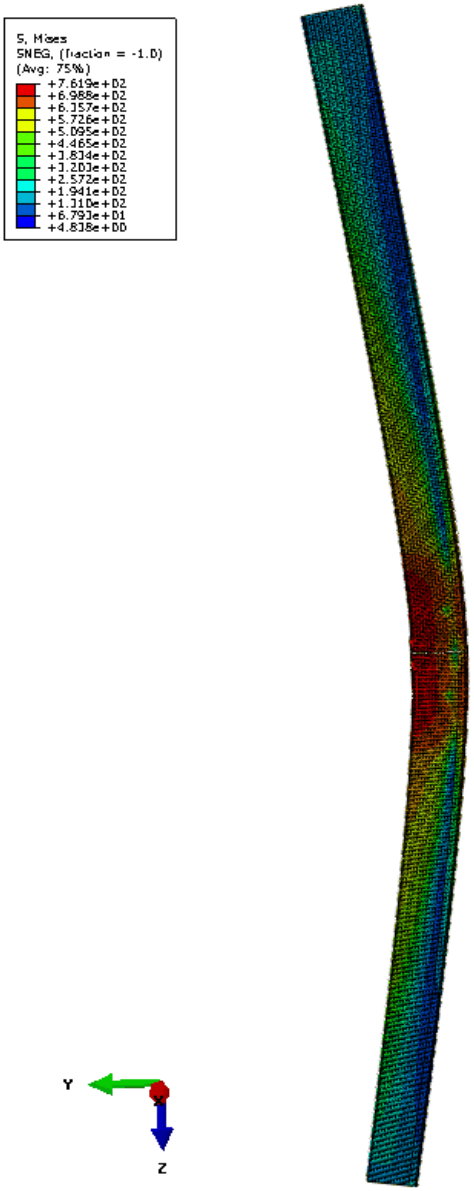

Figure 7 Example of a finite element model of square hollow section made from steel B (S700MC) at 500°C from ABAQUS

6 Results and analysis

In the previous section, the validation exercise showed that the FE model can reasonably predict the behaviour of columns made from HSS grade S460N and S690Q at ambient temperature as well as conventional steel grade S355 at elevated temperature. Therefore, in this section, the model is used to study the buckling behaviour of columns made from high strength steel, at elevated temperature, and recommend guidance for design. As mentioned in Section 4, there are no available test results for HSS columns in fire. In the following sections, the current design rules given in the Eurocode are briefly described and then compared with results from the parametric study.

The current design rules in Eurocode 3 Part 1-2 [14] are mainly based on the work by Talamona *et al.* [11] and Franssen *et al.* [12] on H and I-section columns made from conventional steel grades. The applicability of the Eurocode rules was extended to steels with yield strengths up to 700 N/mm^2 without any additional rules for HSS, as specified in Eurocode 3 Part 1-12 [1]. The design guidelines are summarised, hereafter.

6.1 Cross-section classification

In classifying cross-sections at room temperature in accordance with Eurocode 3, the material factor (ε) given in Eq. 6 for carbon steel is used to allow for variations in the material yield strength $f_{y,20}$:

$$\varepsilon = \sqrt{\frac{235}{f_{y,20}}} \tag{6}$$

At elevated temperature, a reduction factor of 0.85 is applied to ε, as shown in Eq. 7, to account for the decline in strength ($k_{y,\theta}$) and stiffness ($k_{Ea,\theta}$) in a fire situation:

$$\varepsilon = \sqrt{\frac{k_{E,\theta}}{k_{y,\theta}}}\sqrt{\frac{235}{f_{y,20}}} \cong 0.85\sqrt{\frac{235}{f_{y,20}}} \tag{7}$$

The variation in $(k_{E,\theta}/k_{y,\theta})^{0.5}$ as a function of temperature is presented in Fig. 8 for steels A (S690QL) and B (S700MC) [20], as well as the corresponding Eurocode values [14], determined from the recommended reduction factors. From this figure, it can be seen that 0.85 is generally conservative for these HSS grades and can be considered as an additional safety factor. For steels A (S690QL) and B (S700MC) the variation of $(k_{E,\theta}/k_{y,\theta})^{0.5}$ is close to unity until around 450-500°C. At temperatures greater than 500°C, $(k_{E,\theta}/k_{y,\theta})^{0.5}$ is greater than unity and thus the cross-section classification may not change but will improve. This highlights the fact that 0.85 may be too conservative for members made from HSS and could result in underestimating the overall buckling resistance. Based on the reduction factors for steels A (S690QL) and B (S700MC), an appropriate value for cross-section classification of HSS columns would be 0.95. However, due to the inherent variability in material properties resulting from the differences in chemical composition and production route it may be more appropriate to directly incorporate the material strength and stiffness reduction factors (i.e. $(k_{E,\theta}/k_{y,\theta})^{0.5}$) rather than generalise to a single value of 0.85.

Following the Eurocode approach, the cross-section classification of a square hollow section with dimensions 100 × 100 × 4 made from steels A (S690QL) and B (S700MC), at elevated temperature,

changes from Class 3 to Class 4, owing to the reduction factor in Eq. 7. Similarly, a 100 × 50 × 4 rectangular hollow section also changes from Class 3 to Class 4. On the other hand, the Class 1 sections assessed in the parametric study (i.e. 100 × 100 × 5.6 SHS and 100 × 5.0 × 5.6 RHS) retain their Class 1 classification.

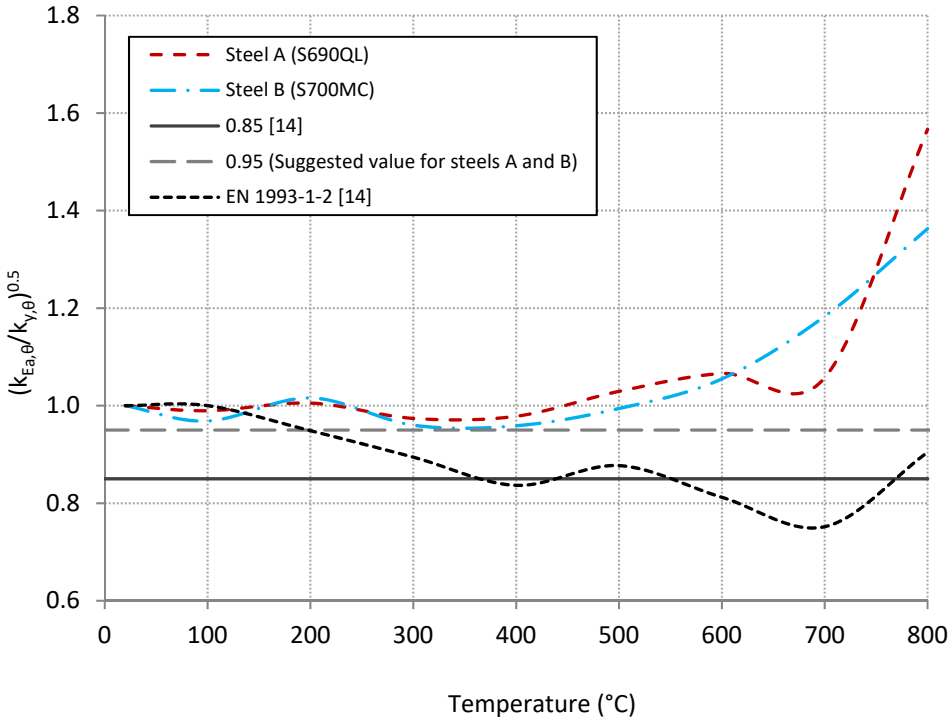

Figure 8 Variation of $(k_{E,\theta}/k_{y,\theta})^{0.5}$ reduction factors with temperature

6.2 Stability of compression members

In accordance with Eurocode 3 Part 1-2 [14], the design buckling resistance ($N_{b,fi,t,Rd}$) of a compression member with Class 1, Class 2 or Class 3 cross-section with uniform temperature θ is determined as:

$$N_{b,fi,t,Rd} = \frac{\chi_{fi} A k_{y,\theta} f_{y,20}}{\gamma_{M,fi}} \quad (8)$$

where A is the gross cross-sectional area of the structural member, $k_{y,\theta}$ is the reduction factor for the effective yield strength presented in Section 2.5, $f_{y,20}$ is the yield strength at ambient temperature, $\gamma_{M,fi}$ is the partial safety factor for fire situation which is taken as 1.0, in accordance with the recommendations in Eurocode 3 Part 1-2 [14], and χ_{fi} is the reduction factor for flexural buckling in the fire design situation given by Eq. 9:

$$\chi_{fi} = \frac{1}{\varphi_\theta + \sqrt{\varphi_\theta^2 - \bar{\lambda}_\theta^2}} \quad (9)$$

In this expression, φ_θ is determined from Eq. 10, whilst the imperfection factor α is found from Eq. 11:

$$\varphi_\theta = \frac{1}{2}\left[1 + \alpha\bar{\lambda}_\theta + \bar{\lambda}_\theta^2\right] \quad (10)$$

$$\alpha = 0.65\sqrt{\frac{235}{f_{y,20}}} \tag{11}$$

In these equations, $\bar{\lambda}_\theta$ is the non-dimensional slenderness at temperature θ as defined by Eq. 12, $\bar{\lambda}$ is the non-dimensional slenderness at ambient temperature and $k_{Ea,\theta}$ is the reduction factor for the elastic modulus at temperature θ.

$$\bar{\lambda}_\theta = \bar{\lambda}\sqrt{\frac{k_{y,\theta}}{k_{E_a,\theta}}} \tag{12}$$

For Class 4 sections, where local buckling instabilities must be considered, a similar approach to ambient temperature design can be used. The cross-sectional area A and reduction factor $k_{y,\theta}$ in Eqs. 8 and 12 are replaced by the reduced effective area A_{eff} and the reduction factor for the 0.2% proof strength $k_{0.2p,\theta}$ presented in Eq. 13, as specified in Appendix E of Eurocode 3 Part 1-2 [14]. However, the critical temperature for Class 4 sections is limited to 350°C which has been shown to be overly conservative and could be improved [45].

$$\bar{\lambda}_\theta = \bar{\lambda}\sqrt{\frac{k_{0.2p,\theta}}{k_{E_a,\theta}}} \tag{13}$$

The aforementioned equations (9-12) are used to produce buckling curves for fire scenarios for Class 1-3 cross-sections, which are presented in Fig. 9. It should be noted that the buckling curves at elevated temperature differ from those presented in Eurocode 3 Part 1-1 [26], for the design of steel structures at ambient temperature, which is presented in Fig. 10 for reference. Firstly, at elevated temperature, there is no plateau in the buckling curve (i.e. at low values of $\bar{\lambda}_\theta$). In addition, at ambient temperature, five different buckling curves (a_0, a, b, c and d) are provided in the code, where the choice of appropriate buckling curve is dependent on the yield strength, geometry of the cross-section, manufacturing process (e.g. hot finished or cold formed) and the buckling axis. On the other hand, the elevated temperature buckling curves are dependent on the yield strength at ambient temperature ($f_{y,20}$) as shown in Fig. 9. In this figure, the buckling curves for S275 and S460 are derived using the reduction factors in Eurocode 3 Part 1-2 [14] whilst the curves for steels A (S690QL) and B (S700MC) utilise the reduction factors derived during an extensive experimental programme [20]. It can be seen that the buckling coefficient increases with (nominal) yield strength as mentioned by Talamona *et al.* [11] and Franssen *et al.* [12]. It should be noted that the use of $\bar{\lambda}_\theta$ defined in Eq. 12 allows for all buckling curves at temperature θ to be represented by a single curve for a given yield strength.

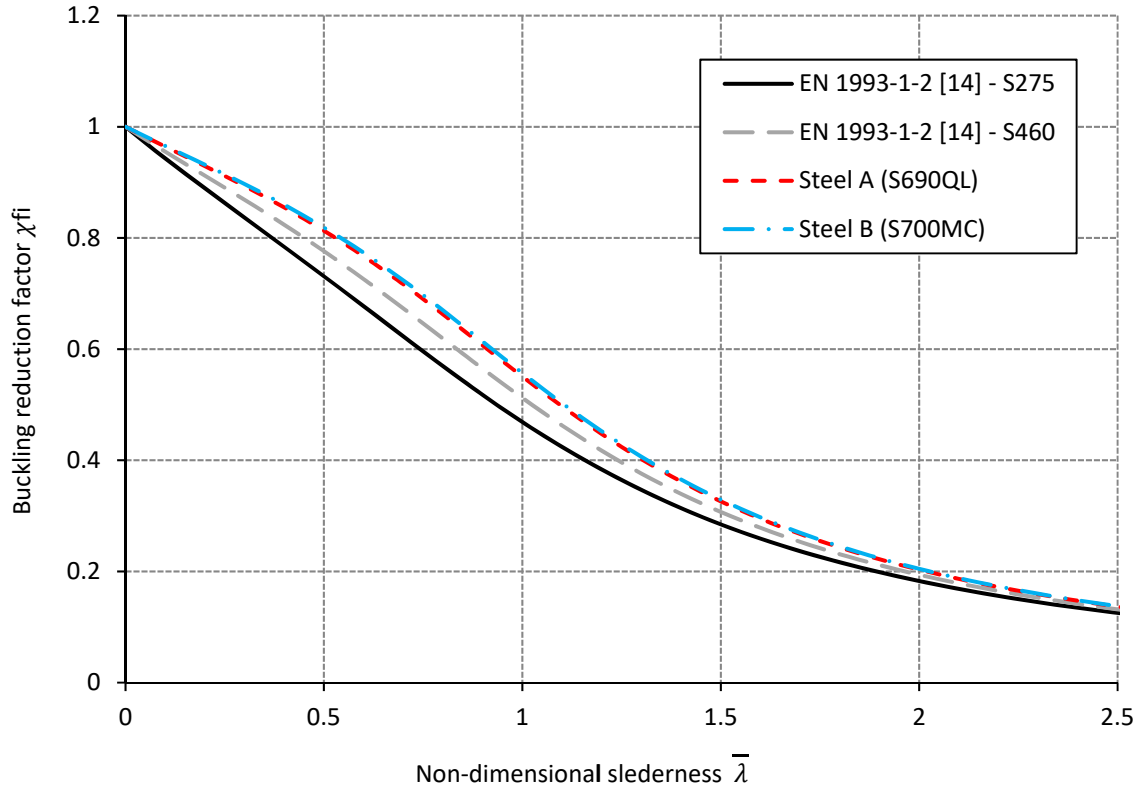

Figure 9: Buckling curves for different steel grades

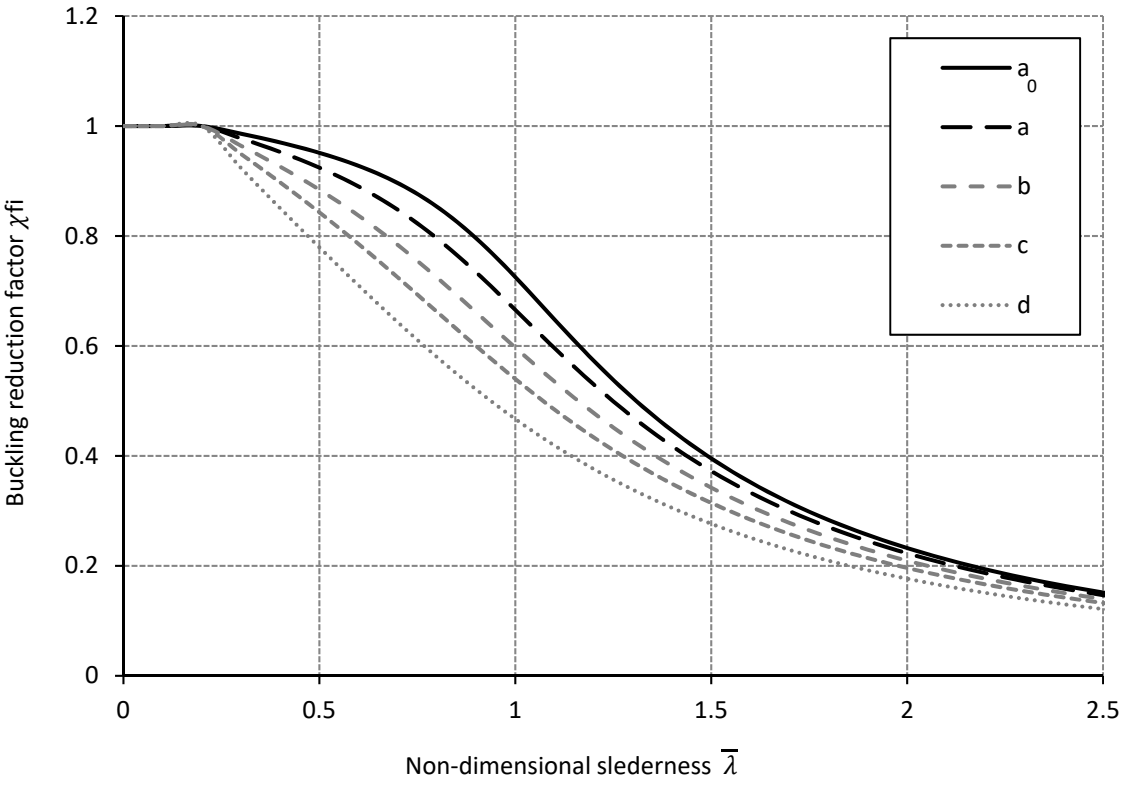

Figure 10: Buckling curves in accordance with EN 1993 Part 1-1 [26]

6.3 Results

This section presents a comparison of the results from the parametric studies with the recommendations in Eurocode 3 Part 1-2 [14] outlined previously. For Class 1 SHS and RHS columns, the buckling reduction factor χ_{fi} is calculated by normalising the ultimate buckling load obtained from the FE models by the 'squash' load $Af_{y,\theta}k_{y,\theta}$ and the non-dimensional slenderness $\bar{\lambda}_\theta$ is calculated using Eq. (12). Since the Class 3 classification changes to Class 4 when taking into account the reduced value ε mentioned in Eq. (7), the ultimate buckling load is normalised by $A_{eff}f_{0.2p,\theta}k_{0.2p,\theta}$ and the non-dimensional slenderness $\bar{\lambda}_\theta$ is calculated using Eq. (13). The reduction factors ($k_{y,\theta}$ and $k_{0.2p,\theta}$) from a previous study [20] were used in the calculations.

The buckling curves and FE results for Class 1 and Class 3 SHS and RHS members made from steel A (S690QL) and B (S700MC), respectively, are presented in Figs. 11 and 12. The buckling coefficients at 100, 200 and 300°C are not presented here, however it is rational to assume that the buckling coefficients will lie between 20 and 400°C. With reference to Fig. 11 (a), the Eurocode buckling curve is generally conservative with respect to the buckling coefficients for steel A (S690QL), with the exception of 800°C at $\bar{\lambda}_\theta$ values below unity. Similarly, in Fig. 11 (b) the Eurocode buckling curve is conservative and adequately predicts the ultimate buckling load for steel B (S700MC) at all temperatures which is related to the better strength and stiffness properties of this material. In Fig. 12 (a), it can be seen that generally, the Eurocode curve is conservative with respect to the buckling coefficients and safely predicts the buckling behaviour of Class 3 sections which change to Class 4 sections at temperatures up to 800°C, even though the Eurocode limits the application of buckling curves for Class 4 sections to temperatures up to 350°C only. There is little disparity between the major and minor buckling axes for RHS sections.

At non-dimensional slenderness values below 1, steel A (S690QL) had higher buckling coefficients and more scatter between the buckling coefficients compared with steel B (S700MC). This is related to the shape of stress-strain curve of the two materials, which strongly influences the stability behaviour of the steel members at low non-dimensional slenderness values ($\bar{\lambda}_\theta$<1.0). For steel B (S700MC), the shape of the stress-strain curve shown in Fig. 4 is non-linear at all temperatures and quite consistent in shape. This is further demonstrated by the strain hardening exponents, n, in Table 2, which are relatively similar at all temperatures, varying between 9.34 and 14.87. However, for steel A (S690QL), the stress-strain response at ambient temperature (20°C) displays an almost bi-linear elastic-plastic response up to the 2% total strain, and shows more non-linear behaviour at higher temperatures as shown in Fig. 3. This is demonstrated by the great disparity between the strain hardening exponents, n, in Table 1, which range from 7.97 to 101.98. The variable degree of nonlinearity of steel A (S690QL) with temperature leads to different buckling responses and hence results in the increased scatter in the obtained results. Members with a non-dimensional slenderness greater than 1.5 buckle elastically, where the average stress falls in the elastic part of the stress-strain curve, and as expected there is little difference in the elevated temperature buckling strength of columns of steels A (S690QL) and B (S700MC).

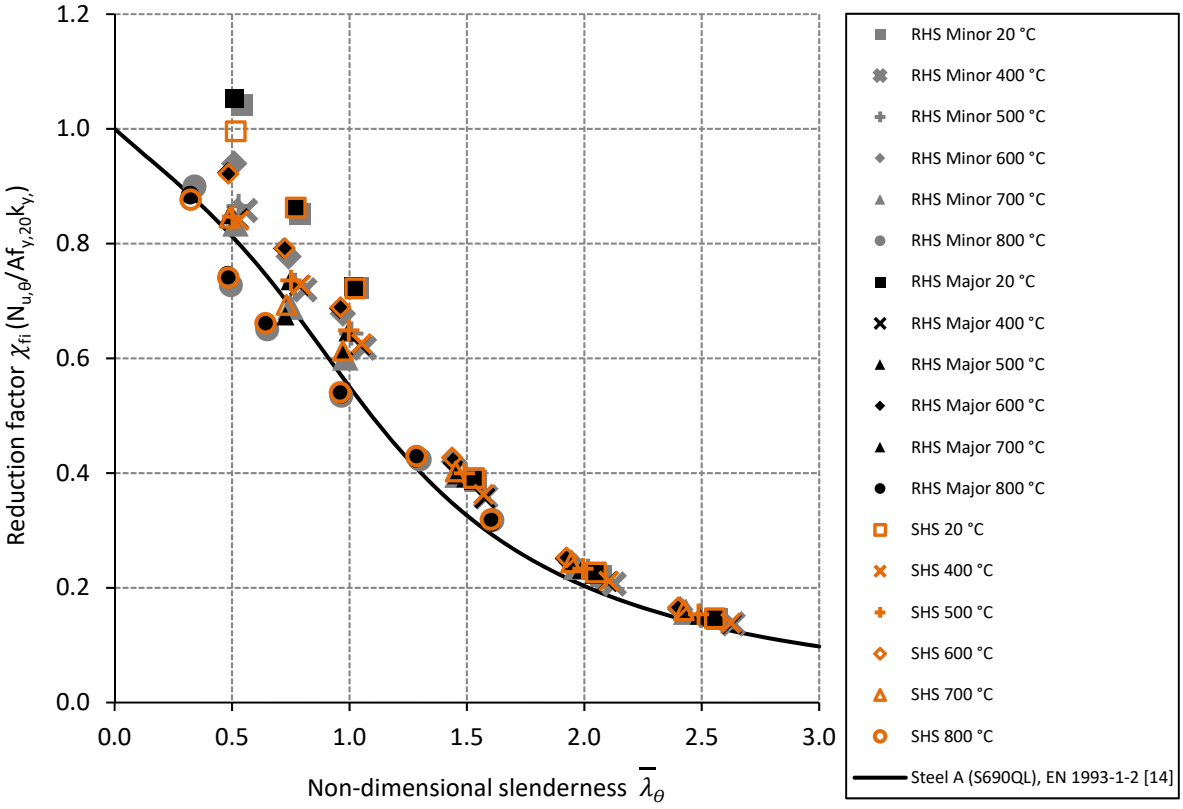

(a)

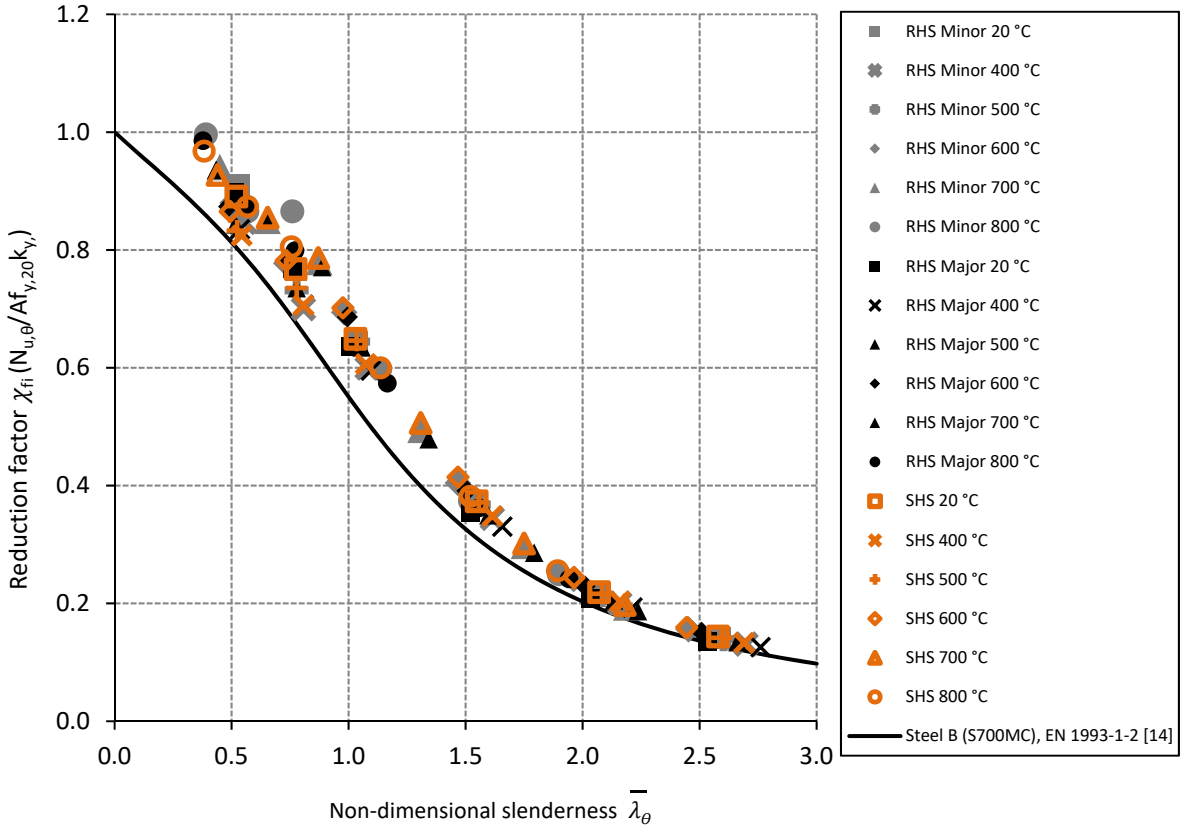

(b)

Figure 11 Comparison of EN 1993-1-2 buckling curve and FE results for Class 1 SHS and RHS (a) A (S690QL) and (b) steel B (S700MC)

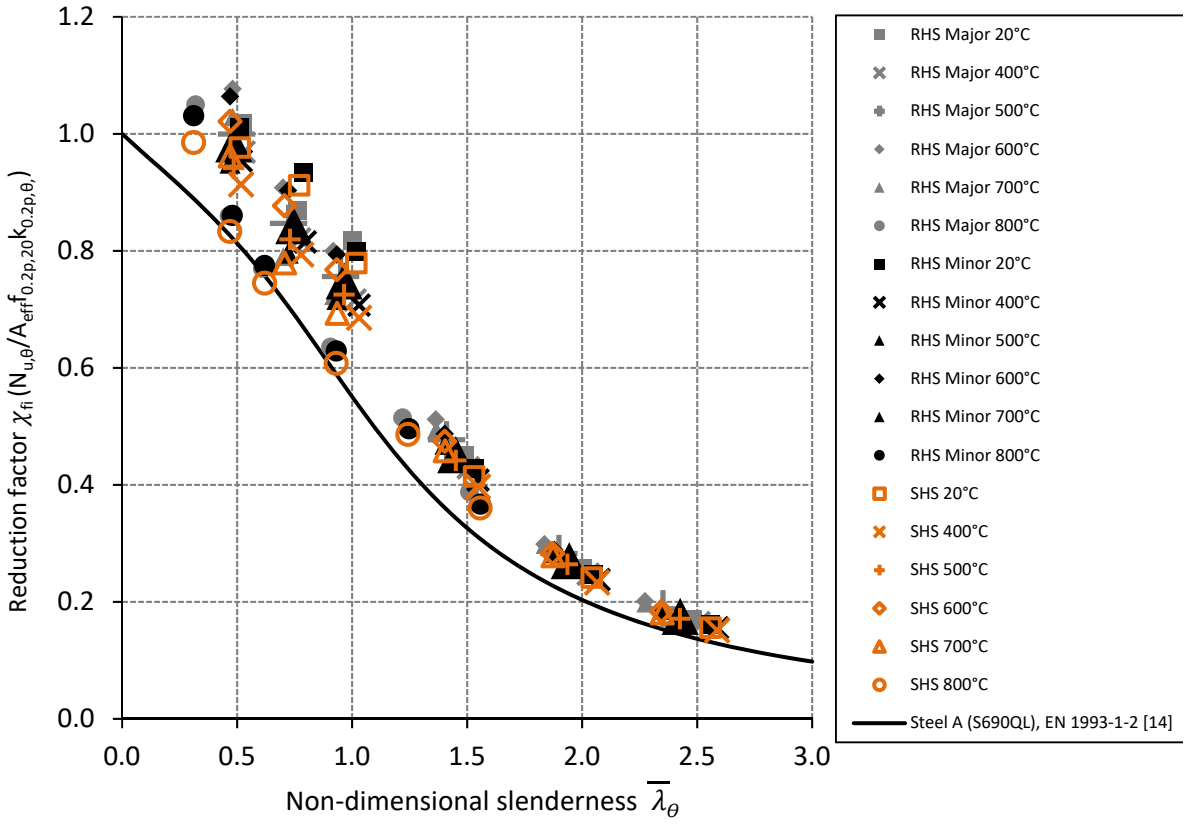

(a)

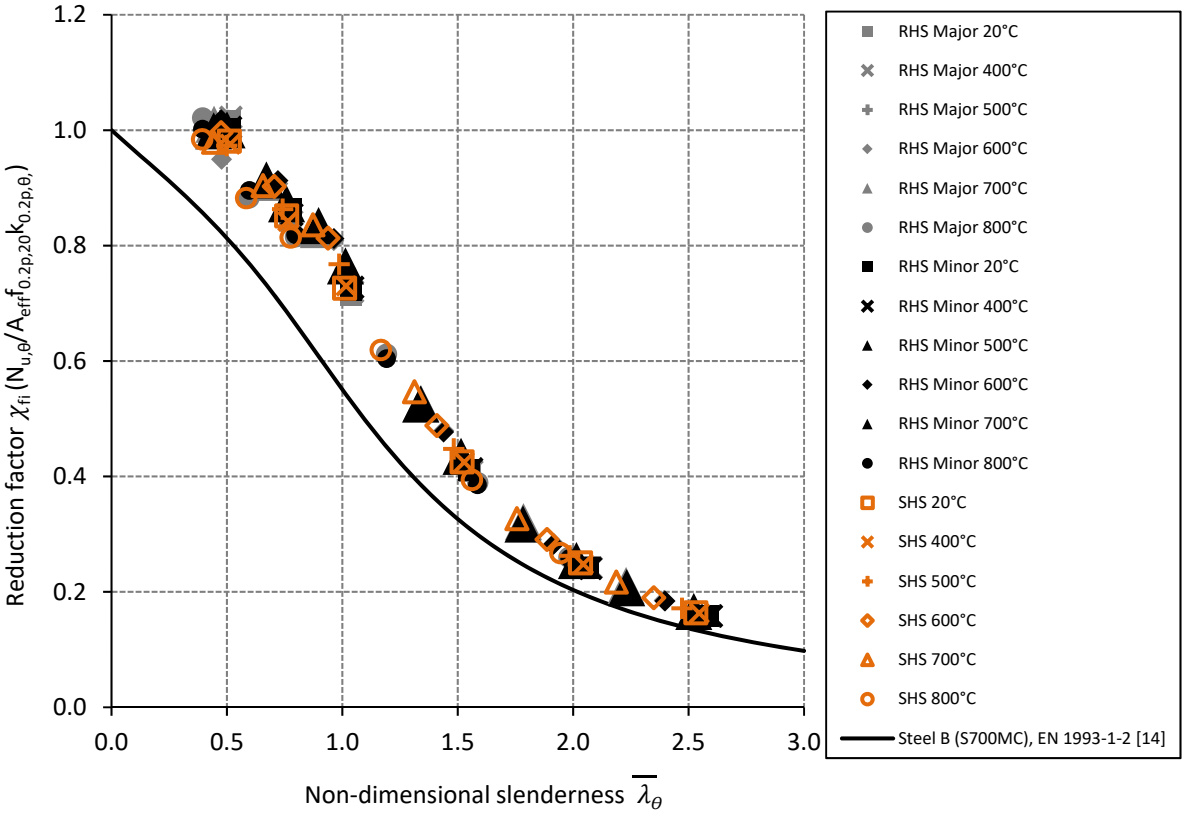

(b)

Figure 12 Comparison of EN 1993-1-2 buckling curve and FE results for Class 3 SHS and RHS (a) steel A (S690QL) and (b) steel B (S700MC)

6.4 Strength parameter

In the assessment of column buckling at elevated temperatures according to Eurocode 3 Part 1-2 [14], the effective yield strength ($f_{y,\theta}$), which is the strength corresponding to 2% strain, and the 0.2% proof strength ($f_{0.2p,\theta}$) are specified in the calculations for Class 1 – 3 and Class 4 cross-sections, respectively. It should be noted that the use of the stress at 2% total strain ($f_{y,\theta}$) in the analysis reflects the large strains (in excess of 2%) observed in standard fire tests on steel structural beams [45]. In steel columns, failure strains in standard fire tests are typically in the order of 1%. However, since the difference between using the strength at 1% and 2% on the overall fire resistance time is marginal, the strength at 2.0% is specified in the analysis for all structural members including beams and columns. The buckling behaviour of columns is controlled by material stiffness which, depending on the non-linearity of the stress-strain response, reduces significantly beyond the 0.2% proof strength. Hence, it is believed that the 0.2% proof strength is a more appropriate parameter for predicting the buckling resistance of columns of all cross-section classes.

Fig. 13 presents the reduction factor for flexural buckling χ_{fi} for Class 1 columns derived by normalising the column failure load from the parametric study by $Af_{0.2p,20}k_{0.2p,\theta}$ rather than $Af_{y,20}k_{y,\theta}$, with the Eurocode curve also depicted. Comparing Fig. 13 (a) and (b) to Fig. 11 (a) and (b), it is evident that by normalising the column failure loads by $Af_{0.2p,20}k_{0.2p,\theta}$ rather than $Af_{y,20}k_{y,\theta}$, the data for different temperatures approximately converge into one curve, which is more prominent for steel A (S690QL), and avoids the requirement for temperature-dependent buckling curves. Furthermore, it is shown that the current Eurocode approach [14] is suitable for steel B (S700MC), whereas a slightly lower curve would be more appropriate for steel A (S690QL).

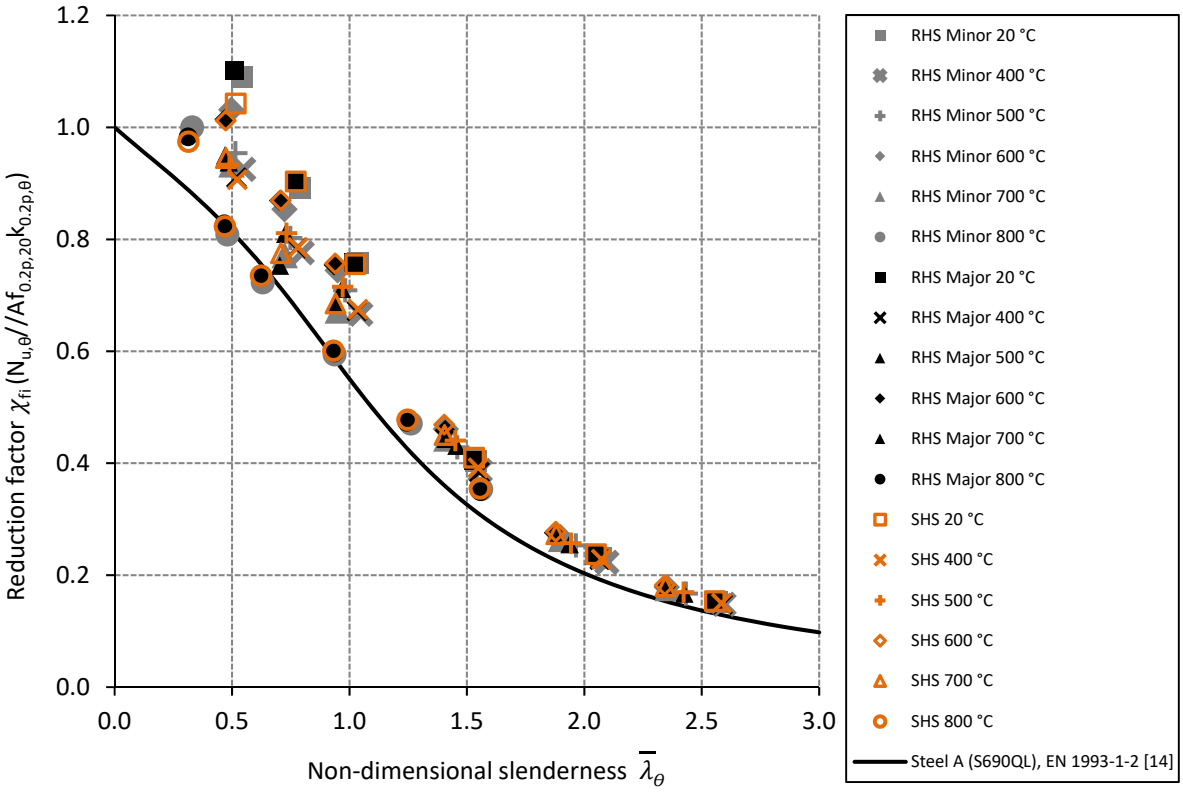

(a)

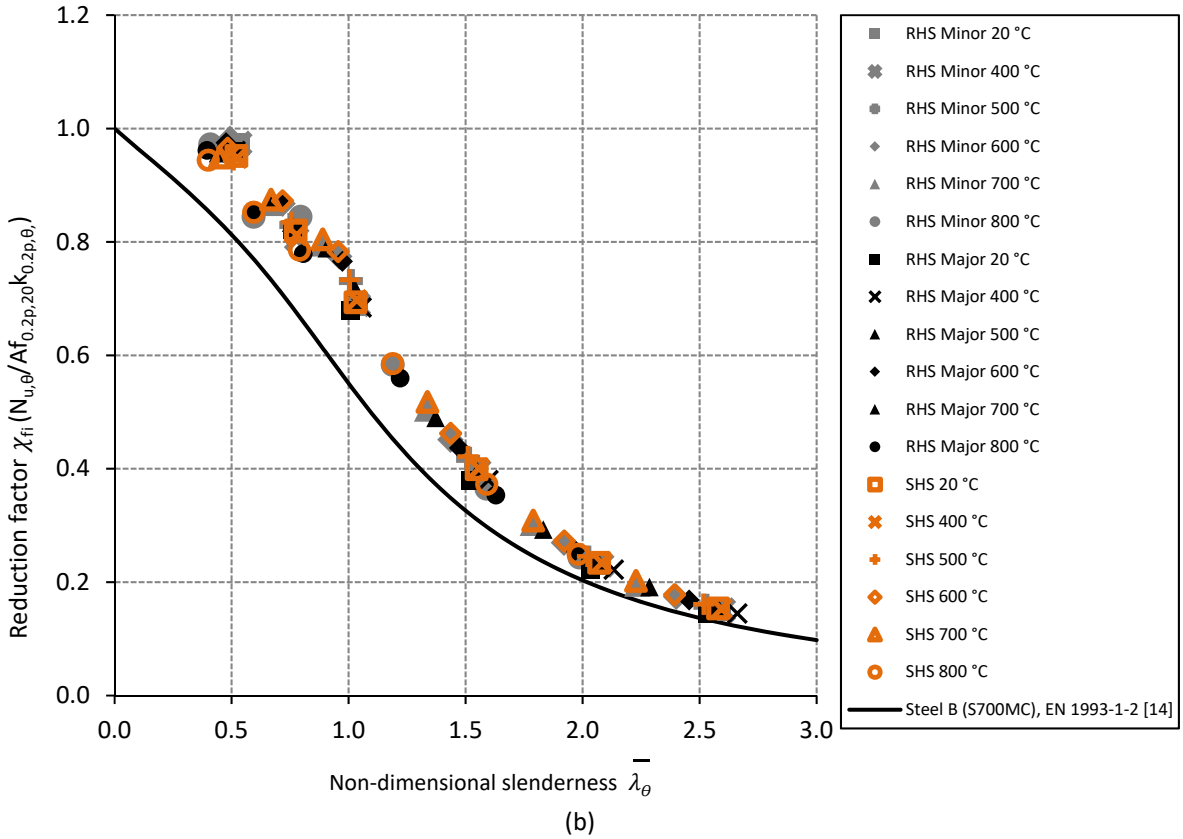

(b)

Figure 13 Comparison of EN 1993-1-2 buckling curve and FE results for Class 1 SHS and RHS normalised by $Af_{0.2p,20}k_{0.2p,\theta}$ for (a) steel A (S690QL) and (b) steel B (S700MC)

7 Conclusions

In this paper, the stress-strain responses of two HSS grades (S690QL and S700MC) are described using the modified Ramberg-Osgood model proposed by Gardner and Nethercot [19], which is shown to closely simulate the stress-strain response. Following this, a numerical study investigating the flexural behaviour of HSS columns, including a detailed description of the FE model and validation results in ABAQUS, is presented, taking into account material properties and geometric imperfections. Once validated, the model is used to perform parametric studies on the behaviour of S690QL and S700MC steel columns at elevated temperature, incorporating the measured stress-strain responses. The results from the parametric studies have been analysed and it is shown that the Eurocode generally provides conservative results with respect to the buckling coefficients and safely predicts the buckling resistance of S700MC, while a lower buckling curve may be needed for S690QL. Minimal difference was observed between buckling about the major and minor axis, which was similarly reported elsewhere [12]. It is also shown that the shape of the stress-strain response, in particular the curvature of the stress-strain response before reaching the 0.2% proof strength, as described by the strain hardening exponent (n), strongly influences the stability behaviour of the steel members at low non-dimensional slenderness values ($\bar{\lambda}_\theta$<1.0). In such scenarios, a higher strain hardening exponent results in better buckling behaviour because the reduction of stiffness occurs at much higher strength. In addition, it is shown in this paper that the 0.2% proof strength rather than the stress at 2% total strain is a better parameter for deriving buckling curves in fire, as the results converge into one curve, negating the need for temperature dependent buckling curves.

Acknowledgements

The financial support provided by the Engineering and Physical Sciences Research Council (EPSRC) and TWI Ltd for the work described in this paper is gratefully acknowledged.

References

[1] CEN, EN 1993-1-12: Eurocode 3. Design of steel structures – Part 1–12 :Additional rules for the extension of EN 1993 up to steel grades S 700, (2007).

[2] European Commission, Rules on high strength steel (RUOSTE) Final Report, Brussels, Belgium, 2016.

[3] European Commission, High strength long span structures (HILONG) Final Report, Brussels, Belgium, 2017.

[4] J. Wang, S. Afshan, M. Gkantou, M. Theofanous, C. Baniotopoulos, L. Gardner, Flexural behaviour of hot-finished high strength steel square and rectangular hollow sections, J. Constr. Steel Res. 121 (2016) 97–109. doi:10.1016/j.jcsr.2016.01.017.

[5] G. Shi, H. Ban, F.S.K. Bijlaard, Tests and numerical study of ultra-high strength steel columns with end restraints, J. Constr. Steel Res. 70 (2012) 236–247. doi:10.1016/j.jcsr.2011.10.027.

[6] H. Ban, G. Shi, Y. Shi, M.A. Bradford, Experimental investigation of the overall buckling behaviour of 960 MPa high strength steel columns, J. Constr. Steel Res. 88 (2013) 256–266. doi:10.1016/j.jcsr.2013.05.015.

[7] F. Javidan, A. Heidarpour, X. Zhao, H. Fallahi, Fundamental behaviour of high strength and ultra-high strength steel subjected to low cycle structural damage, Eng. Struct. 143 (2017) 427–440. doi:10.1016/j.engstruct.2017.04.041.

[8] F. Hu, G. Shi, Y. Shi, Experimental study on seismic behavior of high strength steel frames: Global response, Eng. Struct. 131 (2017) 163–179. doi:10.1016/j.engstruct.2016.11.013.

[9] H. Varol, K.A. Cashell, Numerical modelling of high strength steel beams at elevated

temperature, Fire Saf. J. 89 (2017) 41–50. doi:10.1016/j.firesaf.2017.02.005.
[10] BSI, BS 9999 Fire safety in the design, management and use of buildings – Code of practice, (2017).
[11] D. Talamona, J.M. Franssen, J.B. Schleich, J. Kruppa, Stability of steel columns in case of fire: Numerical Modeling, J. Struct. Eng. 123 (1997) 713–720.
[12] J.-M. Franssen, D. Talamona, J. Kruppa, L.G. Cajot, Stability of Steel Columns in Case of Fire: Experimental Evaluation, J. Struct. Eng. 124 (1998) 158–163. doi:10.1061/(ASCE)0733-9445(1998)124:2(158).
[13] J. Pauli, D. Somaini, M. Knobloch, M. Fontana, Experiments on Steel under Fire Conditions, 2012. http://e-collection.library.ethz.ch/eserv/eth:6696/eth-6696-01.pdf.
[14] CEN, EN 1993-1-2: Eurocode 3. Design of steel structures – Part 1–2: General rules – Structural fire design, (2005).
[15] J. Chen, B. Young, Design of high strength steel columns at elevated temperatures, J. Constr. Steel Res. 64 (2008) 689–703. doi:10.1016/j.jcsr.2007.09.004.
[16] W. Wang, Y. Ohmiya, G. Ma, Fire Resistance Study of Axially Loaded High Strength Steel Columns, Procedia Eng. 62 (2013) 690–701. doi:10.1016/j.proeng.2013.08.115.
[17] R. Ebel, C. Scandella, M. Fontana, M. Knobloch, Member buckling of high strength steel in fire, in: Proc. Int. Colloq. Stab. Ductility Steel Struct., Weinheim, Timisoara, Romania, 2016: pp. 485–492.
[18] D.A. Winful, K.A. Cashell, A.M. Barnes, R.J. Pargeter, High Strength Steel in Fire, in: First Int. Conf. Struct. Saf. under Fire Blast CONFAB 2015, Glasgow, 2015: pp. 105–114.
[19] L. Gardner, D. Nethercot, Experiments on stainless steel hollow sections-Part 1: Material and cross-sectional behaviour, J. Constr. Steel Res. 60 (2004) 1291–1318. doi:10.1016/j.jcsr.2003.11.006.
[20] D.A. Winful, K.A. Cashell, S. Afshan, A.M. Barnes, R.J. Pargeter, Elevated temperature material behaviour of high-strength steel, Proc. Inst. Civ. Eng. - Struct. Build. (2017) 1–11.
[21] Dassault Systèmes, Abaqus 6.14 Online Documentation, (2014).
[22] Y.D. Morozov, O.N. Chevskaya, G. a. Filippov, a. N. Muratov, Fire-resistant structural steels, Metallurgist. 51 (2007) 356–366. doi:10.1007/s11015-007-0067-4.
[23] W. Sha, F.S. Kelly, Z. Guo, Microstructure and Properties of Nippon Fire-Resistant Steels, 8 (1999) 606–612. doi:10.1007/s11665-999-0017-3.
[24] H.K.D.H. Bhadeshia, R. Honeycombe, Steels: microstructure and properties: microstructure and properties, 2nd ed., Edward Arnold, London, 1995.
[25] W. Bolton, R.A. Higgins, Materials for Engineers and Technicians, Routledge, 2014.
[26] CEN, EN 1993-1-1:2005: Eurocode 3. Design of steel structures – Part 1–1: General rules and rules for buildings, 3 (2005).
[27] K.W. Poh, W. Poh, Stress-strain temperature relationship for structural steel, (2001) 371–379.
[28] A. Rubert, P. Schaumann, Structural steel and plane frame assemblies under fire action, Fire Saf. J. 10 (1986) 173–184. doi:10.1016/0379-7112(86)90014-7.
[29] Y. Wang, I. Burgess, F. Wald, M. Gillie, Performance-based fire engineering of structures, CRC Press, 2012.
[30] R. Schneider, J. Lange, Constitutive equations of structural steel S460 at high temperatures, in: Nord. Steel '09 Constr. Conf., 2009: pp. 204–211.
[31] I.-R. Choi, K.-S. Chung, D.-H. Kim, Thermal and mechanical properties of high-strength structural steel HSA800 at elevated temperatures, Mater. Des. 63 (2014) 544–551. doi:10.1016/j.matdes.2014.06.035.
[32] M.X. Xiong, J.Y.R. Liew, Mechanical properties of heat-treated high tensile structural steel at elevated temperatures, Thin-Walled Struct. 98 (2016) 169–176. doi:10.1016/j.tws.2015.04.010.
[33] J.L. Ma, T.M. Chan, B. Young, Material properties and residual stresses of cold-formed high strength steel hollow sections, J. Constr. Steel Res. 109 (2015) 152–165.

doi:10.1016/j.jcsr.2015.02.006.
[34] W. Ramberg, W. Osgood, Description of Stress-Strain Curves By Thee Parameters, NACA Tech. Note. No. 902. (1943).
[35] H.N. Hill, Determination of Stress–Strain Relations from the Offset Yield Strength Values, Washington, 1944.
[36] E. Mirambell, E. Real, On the calculation of deflections in structural stainless steel beams: an experimental and numerical investigation, J. Constr. Steel Res. 54 (2000) 109–133. doi:10.1016/S0143-974X(99)00051-6.
[37] K.J.R. Rasmussen, Full-range stress–strain curves for stainless steel alloys, 59 (2003) 47–61.
[38] S. Afshan, B. Rossi, L. Gardner, Strength enhancements in cold-formed structural sections - Part II: Predictive models, J. Constr. Steel Res. 83 (2013) 177–188. doi:10.1016/j.jcsr.2012.12.007.
[39] J. Buick Davison, I.W. Burgess, R.J. Plank, H. Yu, Y. Hu, Ductility of simple steel connections in fire, Proc. SDSS' Rio 2010 Int. Colloq. Stab. Ductility Steel Struct. 1 (2010).
[40] W.E. Luecke, J.D. McColskey, C.N. McCowan, S.W. Banovic, R.J. Fields, T. Foecke, T. a Siewert, F.W. Gayle, Mechanical properties of structural steels, Federal building and fire safety investigation of the World Trade Center disaster, 2005.
[41] G.M.E. Cooke, An introduction to the mechanical properties of structural steel at elevated temperatures, Fire Saf. J. 13 (1988) 45–54. doi:10.1016/0379-7112(88)90032-X.
[42] J. Wang, L. Gardner, Flexural Buckling of Hot-Finished High-Strength Steel SHS and RHS Columns, J. Struct. Eng. ASCE. 143 (2017) 1–12. doi:10.1061/(ASCE)ST.1943-541X.0001763.
[43] R.G. Dawson, A.C. Walker, Post-buckling of geometrically imperfect plates. Journal of the Structural Division, J. Struct. Div. 98 (1972) 75–94.
[44] L. Twilt, The new eurocode on fire design of steel structures, Seminar. (2001).
[45] R.M. Lawson, G.M. Newman, Structural Fire Design to EC3 & EC4, and comparison with BS 5950, 1996.